Nanotechnology

PAPER

Graphene—vertically aligned carbon nanotube hybrid on PDMS as stretchable electrodes

To cite this article: Junjun Ding *et al* 2017 *Nanotechnology* **28** 465302

IOP Publishing Nanotechnology

Nanotechnology **28** (2017) 465302 (9pp) https://doi.org/10.1088/1361-6528/aa8ba9

Graphene—vertically aligned carbon nanotube hybrid on PDMS as stretchable electrodes

Junjun Ding[1,3], Shichen Fu[1], Runzhi Zhang[1], Eric Boon[2], Woo Lee[2], Frank T Fisher[1] and Eui-Hyeok Yang[1]

[1] Department of Mechanical Engineering, Stevens Institute of Technology, Castle Point on Hudson, Hoboken, NJ 07030, United States of America
[2] Department of Chemical Engineering and Materials Science, Stevens Institute of Technology, Castle Point on Hudson, Hoboken, NJ 07030, United States of America

E-mail: eyang@stevens.edu

Received 2 August 2017, revised 4 September 2017
Accepted for publication 11 September 2017
Published 23 October 2017

Abstract

Stretchable electrodes are a critical component for flexible electronics such as displays, energy devices, and wearable sensors. Carbon nanotubes (CNTs) and graphene have been considered for flexible electrode applications, due to their mechanical strength, high carrier mobility, and excellent thermal conductivity. Vertically aligned carbon nanotubes (VACNTs) provide the possibility to serve as interconnects to graphene sheets as stretchable electrodes that could maintain high electrical conductivity under large tensile strain. In this work, a graphene oxide (GO)-VACNT hybrid on a PDMS substrate was demonstrated. Here, 50 μm long VACNTs were grown on a Si/SiO_2 wafer substrate via atmospheric pressure chemical vapor deposition. VACNTs were directly transferred by delamination from the Si/SiO_2 to a semi-cured PDMS substrate, ensuring strong adhesion between VACNTs and PDMS upon full curing of the PDMS. GO ink was then printed on the surface of the VACNT carpet and thermally reduced to reduced graphene oxide (rGO). The sheet resistance of the rGO-VACNT hybrid was measured under uniaxial tensile strains up to 300% applied to the substrate. Under applied strain, the rGO-VACNT hybrid maintained a sheet resistant of $386 \pm 55\ \Omega/\text{sq}$. Cyclic stretching of the rGO-VACNT hybrid was performed with up to 50 cycles at 100% maximum tensile strain, showing no increase in sheet resistance. These results demonstrate promising performance of the rGO-VACNT hybrid for flexible electronics applications.

Supplementary material for this article is available online

Keywords: flexible electronics, stretchable electrode, carbon nanotubes, graphene, graphene oxide, vertically aligned carbon nanotubes

(Some figures may appear in colour only in the online journal)

1. Introduction

Three-dimensional (3D) carbon structures have been intensively investigated due to their advantageous properties such as high conductivity, large surface area, large accessible pore structure, and their chemical compatibility [1–4]. Based on these properties, 3D carbon materials are being pursued as high performance electrodes for supercapacitors or flexible electronics [5–14]. Hierarchical porous materials especially porous carbon materials with macropores and interconnected meso- and micropores are promising candidates as electrode materials for sensors [15–18], batteries [19], supercapacitors

---

[3] Current address: Kazuo Inamori School of Engineering, New York State College of Ceramics, Alfred University, Alfred, NY 14802, United States of America.

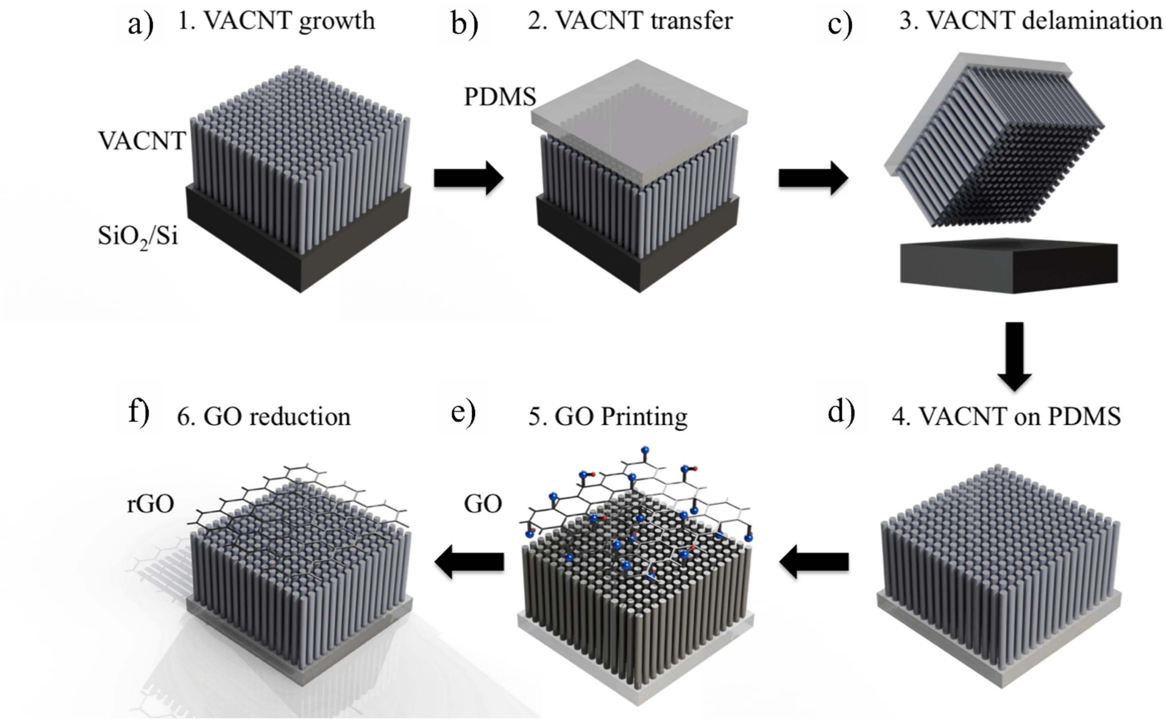

Figure 1. Schematic of fabrication process of rGO-VACNT hybrid on PDMS substrates. (a) A VACNT carpet is grown on a Si/SiO$_2$ substrate via APCVD. (b) The VACNT carpet is then slightly pressed onto the surface of semi-cured PDMS. (c) and (d) once the PDMS with the embedded VACNTs is fully cured, the VACNT-PDMS layer is slowly peeled off from the original Si/SiO$_2$ substrate. (e) GO is inkjet printed on the top of VACNT carpet. (f) The rGO-VACNT hybrid is obtained with thermal reduction of the graphene oxide.

[20–22], and fuel cells [10]. Dual templating, a method where two templates with dimensions at different scales are combined, is widely used to fabricate hierarchical porous carbon [4]. In addition, hierarchical porous carbon materials with high surface area and pore volume have been produced with ice templating, utilizing a colloidal silica hard template [4]. These hierarchical porous carbon materials are promising candidates as electrode materials for an electric double layer capacitor.

Vertically aligned carbon nanotubes (VACNTs) have been widely explored [1, 23–33], owing to their advantages of a high degree of order, good controllability, and easy manipulation [34]. VACNTs can be grown by chemical vapor deposition (CVD) on substrates with pre-deposited catalysts [1, 35]. In contrast to VACNTs on insulating substrates, a graphene-VACNT hybrid provides higher lateral electrical conductivity across the hybrid sheet. To this end, VACNTs and graphene have been combined for constructing stretchable transparent conductors [11, 36, 37], electrode materials for supercapacitors [38–41], Lithium-ion batteries [42], and solar cells [26]. Unlike CVD growth of graphene for graphene-VACNT hybrids, inkjet printing offers fast and low cost fabrication of GO at room temperature (RT) on a large area substrate using GO ink [43–45]. The GO ink can be manufactured in bulk by exfoliating GO in water using sonication, producing a printable GO water solution [46]. The inkjet printed GO can be reduced into reduced graphene oxide (rGO) after the removal of intercalated water molecules and oxide groups including carboxyl, hydroxyl, and epoxy groups.

A key challenge in fabricating graphene (or rGO)-VACNT hybrids toward constructing stretchable electrodes includes the need of transferring or directly synthesizing them on a polymer-based flexible substrate. Due to the high temperature growth conditions of VACNTs, synthesis of VACNTs direct on a flexible substrate (e.g., CVD growth) is generally not feasible. To this end, various transfer methods have been developed to transfer the patterned CNT structures to the target substrates [47–49]. For example, PECVD growth of VACNTs on flexible plastic substrates at relatively low temperature (~250 °C) was reported; however, temperatures above 250 °C led to brittleness of the polymer and substrate curvature [50]. To avoid exposing polymer substrates to the high temperature conditions required for CVD growth, VACNTs were transferred from a Si substrate to a polycarbonate substrate [48]. Additionally, VACNT-polymer hybrid architectures was prepared by impregnating VACNTs into a transparent PDMS film, showing conductance under extreme tensile and compressive strains [49]. While these reported methods demonstrate progress for stretchable electrode applications, they either require high temperature processes during transfer or result in infiltrated polymer remaining within VACNT structures from the transfer process.

Here, we report the fabrication and characterization of a rGO-VACNT-PDMS hybrid structure as a stretchable electrode. We transfer VACNTs to PDMS substrates by placing semi-cured PDMS atop as-grown VACNTs on Si/SiO$_2$ substrates prior to fully curing the PDMS which ensures strong adhesion of PDMS to the top portions of the VACNTs. We

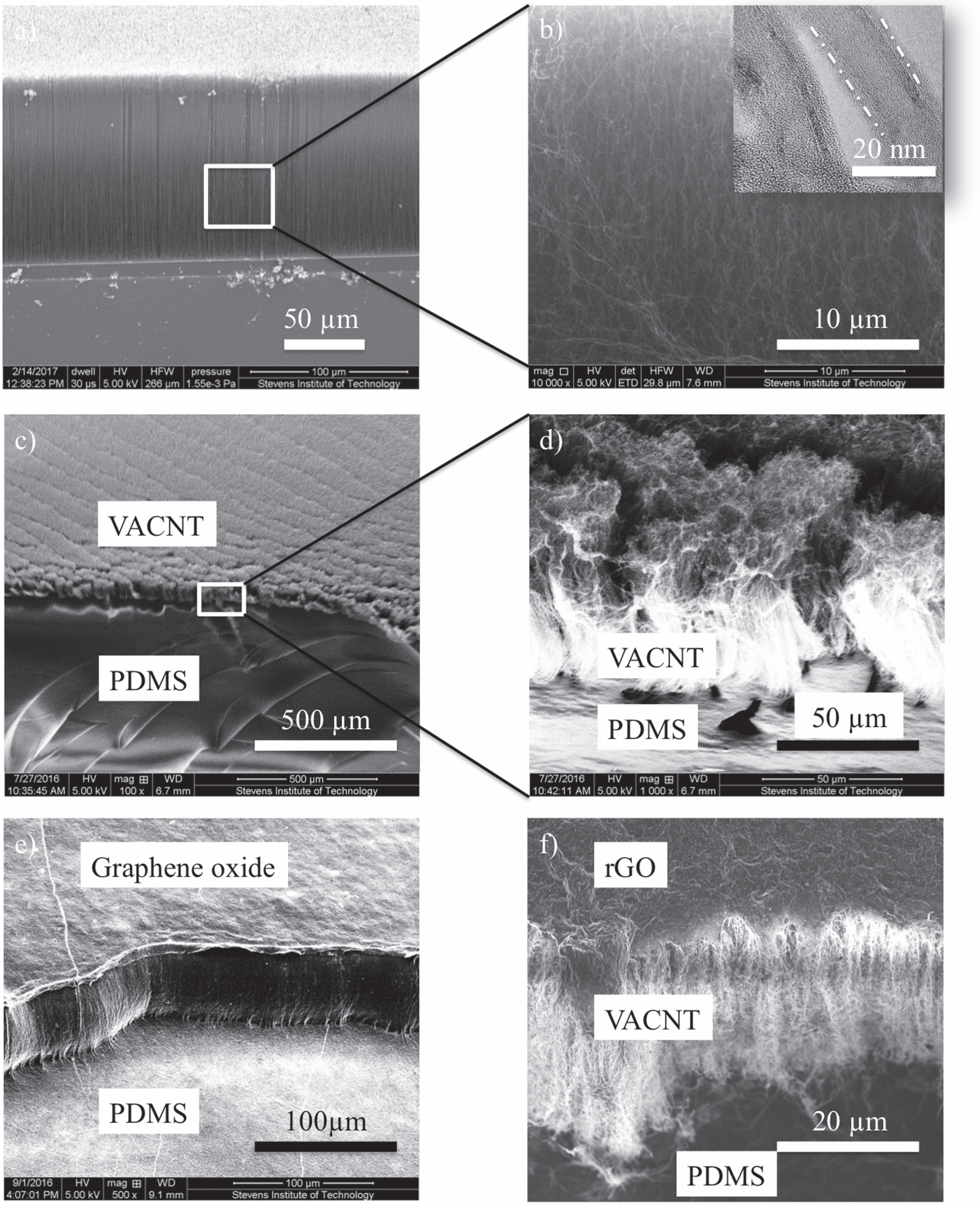

Figure 2. SEM images of (a) and (b) VACNTs grown on SiO_2 substrates via APCVD (inset shows TEM image of multiwall CNTs with a diameter of $\sim$20 nm, with white dashed lines outlining the walls of the multiwall CNT for clarity), (c) and (d) VACNTs on a PDMS substrate obtained by delaminating the VACNT-PDMS stack from the SiO_2 substrate after the top of VACNT carpet is bonded with a pre-cured PDMS, (e) GO atop VACNTs on a PDMS substrate by inkjet printing, (f) reduced GO on top of VACNTs on PDMS substrate after thermal reduction.

then delaminate VACNT-PDMS from the Si substrate from which the VACNTs were grown. GO is then inkjet printed on the top of VACNTs on the PDMS substrate, followed by thermal reduction, to create a rGO-VACNT hybrid. Sheet resistance measurements under up to 300% applied uniaxial tensile trains maintain a sheet resistance of $386 \pm 55\ \Omega/\mathrm{sq}$, with cyclic stretching up to 50 cycles at 100% maximum tensile strain indicate no increase in sheet resistance.

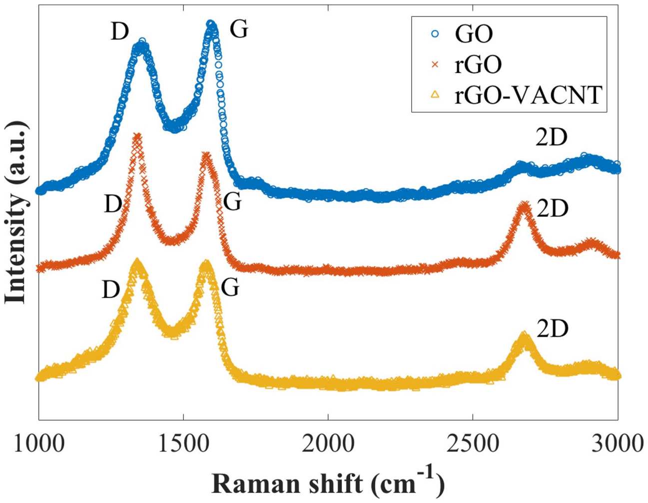

Figure 3. Raman spectra of GO (top line), rGO (middle line), and rGO-VACNT hybrid (bottom line) on PDMS substrates. The peak locations of the Raman spectra are D peak at 1338 cm^{-1}, G peak at 1574 cm^{-1}, and 2D peak at 2677 cm^{-1}. The intensity ratios of the D and G peaks (I_D/I_G) are 0.92 for GO and 1.13 for rGO, respectively.

2. Fabrication

A schematic of the fabrication process to create the rGO-VACNT hybrid on PDMS substrates is shown in figure 1. A VACNT carpet was grown on a Si/SiO_2 wafer substrate via atmospheric pressure chemical vapor deposition (APCVD) (Step 1). First, catalyst layers consisting of 5 nm of aluminum (Al), acting as the supporting layer, and 3 nm of iron (Fe), acting as the catalyst layer, were deposited on a Si/SiO_2 wafer substrate using physical vapor deposition. The substrate with catalyst layer was then placed in an APCVD chamber and heated to 750 °C at a rate of 30 °C min^{-1} with 500 sccm Ar. VACNT growth was conducted at 750 °C for 15 min with 60 sccm H_2 and 100 sccm C_2H_4. The chamber was then cooled down to RT at 30 °C min^{-1} while keeping Ar flowing at the same rate. The resulting VACNTs with ~50 μm height are shown in figure 2. Depending on the growth time, the resulting VACNT carpet has a height ranging from a few microns to more than 100 μm. While the CNTs look vertically aligned at lower magnification, high magnification SEM images (figure 2(b)) show that the CNTs entangle laterally, providing mechanical and electrical interconnection. The transmission electron microscope (TEM) image as an inset in figure 2(b) shows that the VACNT carpet consists of multi-wall CNTs. The average outer diameter of the CNTs is approximately 20 nm, and the average spacing between the CNTs is approximately 50 nm.

To transfer the VACNTs from the Si/SiO_2 wafer substrate to a PDMS substrate (Step 2), a liquid mixture of PDMS base and curing agent (Sylgard 184 Silicone Elastomer, Dow Corning) with a ratio of 10:1 by weight were thoroughly mixed and degassed under reduced pressure using a vacuum pump. The liquid PDMS mixture was then placed on a hot plate at 65 °C for 2 h (the normally required time for full cure is ~4 h). The VACNT carpet on a Si/SiO_2 wafer substrate was then flipped over and placed on top of the semi-cured PDMS. At this stage, the semi-cured PDMS is rigid enough to support the VACNT carpet on the Si/SiO_2 wafer substrate, preventing it from being fully immersed into PDMS. During this transfer, the surface of the semi-cured PDMS strongly adheres to the tips of the VACNTs, which are partially immersed into the semi-cured PDMS. The VACNT carpet was then slightly pressed onto the surface of semi-cured PDMS, making a VACNT-PDMS stack, which was kept at RT for another 4 h to completely cure the PDMS. The PDMS pre-curing step should be precisely controlled to ensure the tip of the VACNT carpet bonds with the surface of PDMS; insufficient pre-curing or over-curing of the PDMS prior to this step results in an unsuccessful transfer process. Specifically, without the pre-curing step, the liquid PDMS completely fills the vacancy around VACNTs when the liquid PDMS mixture is poured onto the VACNTs. On the other hand, if the PDMS is over pre-cured, then there is insufficient bonding between the PDMS and VACNTs, resulting in partial transfer of the VACNTs from the as-grown Si/SiO_2 substrate onto the PDMS substrate.

Delamination of the VACNTs from Si/SiO_2 substrate (Step 3) is the final step of transferring the VACNTs to PDMS. Because of the strong adhesion between the PDMS substrate and the VACNT carpet, the PDMS and VACNTs can be slowly peeled off from the original Si/SiO_2 substrate. The delamination is possible when the adhesion force between the PDMS and the VACNTs is stronger than that between the VACNTs and the Si/SiO_2 substrate. As shown in figures 2(c) and (d) (Step 4), the VACNTs were successfully transferred from Si/SiO_2 to PDMS substrate without collapsing. The low magnification SEM image (figure 2(c)) shows a uniformly transferred VACNT carpet on PDMS, with the CNTs completely removed from the original Si/SiO_2 substrate. High magnification SEM imaging (figure 2(d)) shows that the CNTs were rooted in the PDMS, ensuring strong adhesion between the VACNTs and PDMS substrate.

After transferring as-grown VACNTs from SiO_2 substrate to PDMS, GO was printed on the top of VACNT carpet using an inkjet printer (Step 5). First, GO ink was prepared by dispersing commercial GO (Cheap Tubes Inc.) in water at 2 mg ml^{-1}. The average dimensions of the GO flakes provided by the supplier was 500 nm × 500 nm × 0.8 nm. The GO solution was sonicated for 15 min followed by filtering with a 450 nm Millex syringe filter before loading into a print head cartridge. A commercial Material Printer DMP 2800 inkjet printer (Fujifilm Dimatix) was used to print the GO ink onto the VACNT on PDMS substrate through an array of piezoelectric nozzles. The GO ink droplet produced a disk-shaped GO dot on the substrate as a result of the droplet hitting the substrate and spreading followed by the evaporation of the solvent (water). The island formation largely depends on the hydrophobicity of the printing surface, and more pronounced island formation occurred on hydrophobic surfaces. Thus, prior to the GO printing, VACNTs on PDMS substrates was treated by oxygen plasma at 100 W for 30 s to generate carbon oxide on the top of the VACNT carpet, therefore making the surface more hydrophilic to assist with the printing process. A thin layer (~100 nm) of GO film was

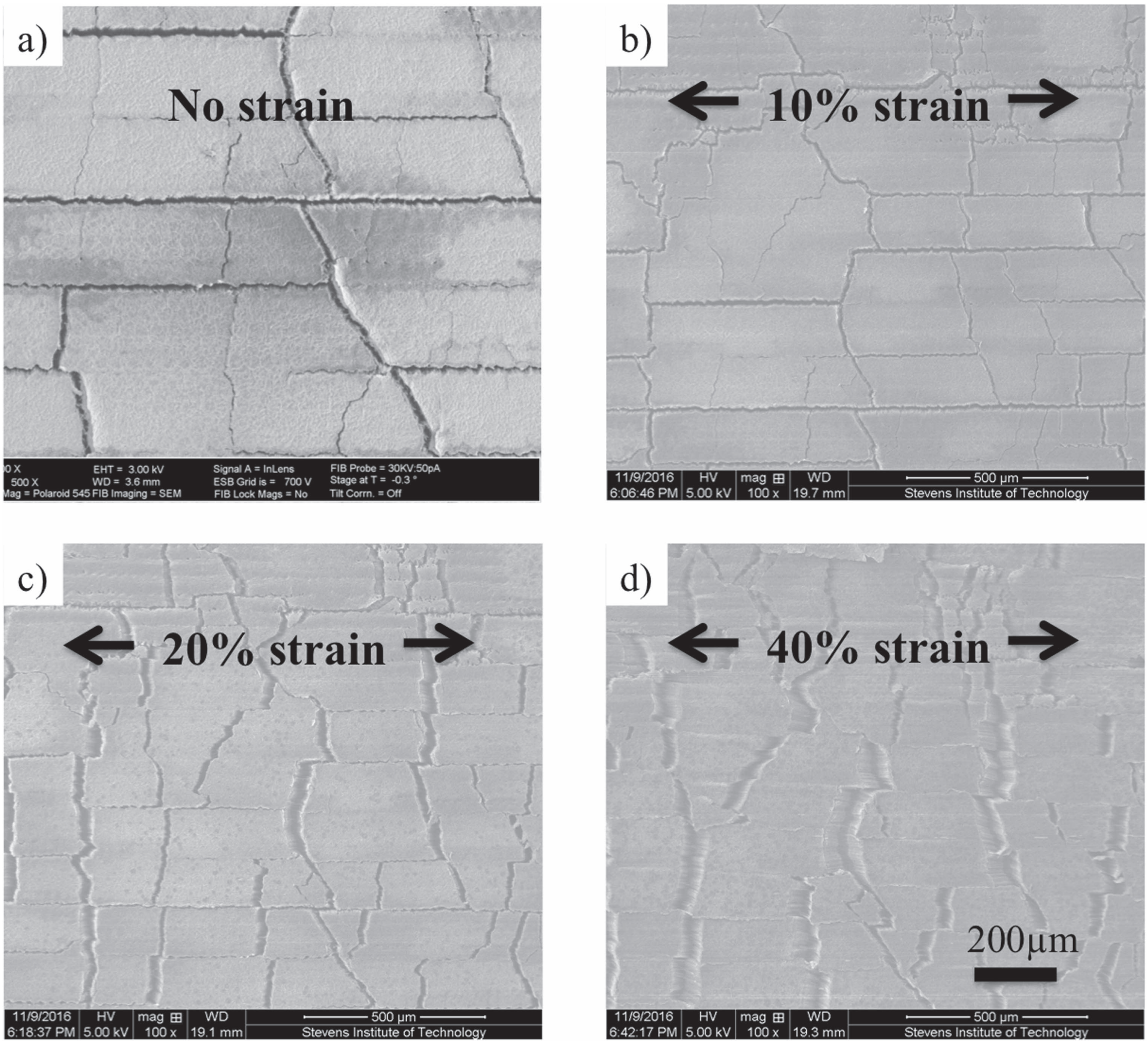

Figure 4. (a)–(d) Top view SEM images of crack formation on the rGO layer of the rGO-VACNT hybrid structure with various tensile strains (0%–40%) applied to the PDMS substrate.

then inkjet printed in a water solution onto the surface of VACNT carpets to interconnect the VACNTs on the topside with graphene oxide (figure 2(e)).

To increase the conductivity of the GO, in Step 6 the GO-VACNT sample was placed in a tube furnace (Microtherm MT, Mellen) at 200 °C for 2 h with flowing nitrogen gas. The thermal reduction process of GO has six important temperature zones: RT—130 °C, 130 °C–180 °C, 180 °C–600 °C, 800 °C–1000 °C, and 1000 °C–2000 °C [51]. Mild and drastic vaporization of water occurs at the first two stages RT—130 °C and 130 °C–180 °C. At the stage 180 °C–600 °C, the removal of main oxide groups in GO effectively reduces the GO into rGO [51]. Meanwhile, the curing temperature strongly affects the mechanical properties of PDMS [52]. The highest usage temperature of PDMS suggested by Dow Corning is 200 °C, while the highest curing temperature of PDMS is 150 °C. The nitrogen gas protected the carbon hybrid material from oxidization and helped to remove water vapor molecules during the GO reduction process. After the thermal reduction of GO at 200 °C for 2 h, a rGO-VACNT hybrid structure on a flexible PDMS substrate was fabricated (figure 2(f)).

3. Characterization and discussion

The Raman spectra of the GO, rGO, and rGO-VACNT hybrid on PDMS substrates are shown in figure 3. The Raman measurements were taken with a Horiba Xplora system with an Andor iDus 420 detector. The Raman spectra were obtained using a 14 mW, 532 nm laser with a spot size of 3 μm, and taken multiple times on different spots of samples. The Raman spectrum of GO (figure 3 (upper line)) shows a D peak at 1338 cm^{-1}, a G peak at 1574 cm^{-1}, and a 2D peak at 2677 cm^{-1}. The prominent D peak is due to the attachment of hydroxyl and epoxide groups on the carbon basal plane, creating the structural imperfection [53]. The Raman spectra of rGO (figure 3 (middle line)) and rGO-VACNT hybrid (figure 3 (lower line)) show no obvious shift of the D and G peaks. The intensity of the D band is related to the size of the in-plane sp^2 domains; therefore the increase of the D peak

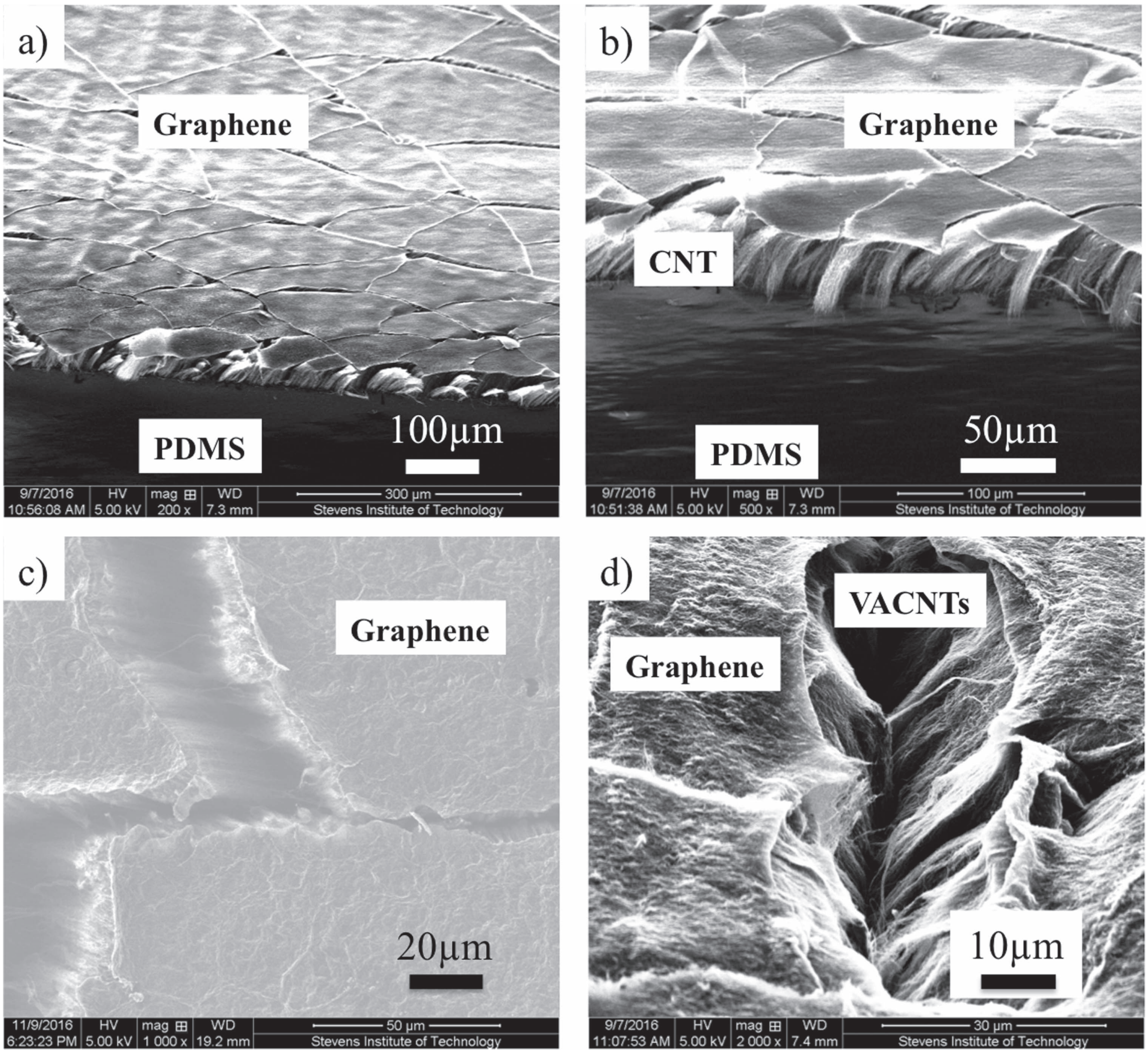

Figure 5. SEM images of cracks in rGO-VACNT hybrid. (a) SEM image of rGO-VACNT hybrid at no tensile strain (45° titled view), (b) SEM image of rGO-VACNT hybrid at no tensile strain (45° titled magnified view), (c) SEM image of rGO-VACNT hybrid with 10% applied tensile strain (top view), and (d) SEM image of rGO-VACNT hybrid under 20% applied tensile strain, showing that the VACNTs remain interconnected (visible in the crack regions).

intensity indicates forming more sp^2 domains [54]. The intensity ratio of the D and G peaks (I_D/I_G) is widely used to measure the efficiency of GO reduction. The intensity ratios are 0.92 for GO and 1.13 for rGO, respectively. The intensity ratio (I_D/I_G) of rGO is higher than that of GO, showing the effective reduction to rGO during the thermal reduction process. The Raman spectrum of rGO and rGO-VACNT show a more pronounced 2D peak than that of the GO, also indicating effective thermal reduction. The widths of these 2D bands are larger in comparison to monolayer graphene, which suggests that multiple layers of the graphene sheets within rGO and rGO-VACNT [55].

Figure 4 shows SEM images of the rGO-VACNT hybrid on a PDMS substrate subject to 0%–40% tensile strain from applied perpendicular to the VACNT forest. Cracks are observed on the rGO layer for the as-fabricated hybrid even without any strain applied to the sample. During the VACNT transfer process and sample handling during GO printing process, twisting, stretching, and bending of the flexible PDMS substrate is inevitable, causing cracks on the rGO layer. With increasing tensile strain applied to the sample, the cracks perpendicular to the stretching direction expanded gradually, while the cracks parallel to the stretching direction appear to compress due to the Poisson effect.

Further examination of the cracks in the rGO film in the rGO-VACNT hybrid is shown in figure 5, cracks are found in the rGO film prior to the application of tensile strain to the PDMS substrate. While handling the flexible PDMS substrate, strain is inevitably applied on the rGO-VACNT, causing cracks in the rGO film. SEM images of the 45° tilted view in figures 5(a) and (b) clearly show cracks (rather than crumpling) on the rGO film. In addition, high magnification SEM images showing a top view of the crack area indicate that the isolated rGO islands remain electrically interconnected with the CNTs underneath, when the rGO-VACNT hybrid is subject to 10% and 20% applied tensile strains as shown in figures 5(c) and (d). Magnified SEM images in figure 2 show that CNTs are wavy and laterally

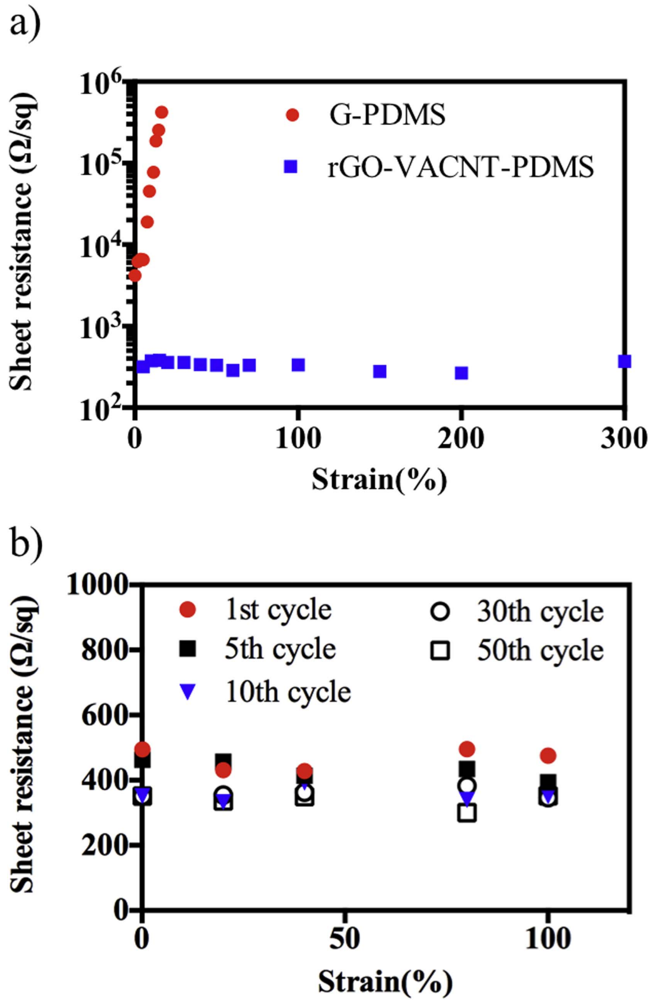

Figure 6. (a) Sheet resistance of the rGO-VACNT hybrid on PDMS and CVD grown graphene on PDMS under tensile strain. (b) Sheet resistance of the rGO-VACNT hybrid on PDMS with cyclic loading up to 100% strain.

interconnected. The wavy CNTs were found to stay interconnected during stretching. Figure 5(d) shows that the CNTs stay connected under 20% tensile strain. The CNT network remains laterally connected with applied tensile strain, ensuring that the rGO-VACNT hybrid remains electrically connected under large values of applied tensile strain.

The sheet resistance of rGO-VACNT hybrid was measured using a four-point probe method by passing current I through the outside two points of the probe from 1 to 100 mA and measuring the voltage V across the two inside points of the probe. The detailed setup can be found in previously published work [6]. The four-point probe head (SP4-62045TBS, Lucas Signatone Corp.) consists of four probes with 1.587 mm spacing between adjacent probes. Because the rGO-VACNT hybrid thickness is around 50 μm and the edges of the hybrid are over four times the spacing distance of the probes, the sheet resistance R_s can be determined based on the simplified equation [56]

$$R_s = 4.53 \cdot V/I.$$

Because the spacing between the four-point probes is much larger than the average size of the rGO cracks, the sheet resistance of the rGO-VACNT hybrid is measured across multiple rGO islands caused by strain (see figure 4) as shown in figure 6. The rGO islands remain electrically interconnected due to the entangled VACNTs underneath the rGO islands as shown in figure 5. The sheet resistances of the rGO-VACNT hybrid on the PDMS substrate under tensile strain are shown in figure 6(a). As a control, the sheet resistance of CVD grown graphene on PDMS (transferred with previously reported PDMS transfer method) [6] is also shown in figure 6(a). The sheet resistance of the rGO-VACNT hybrid on PDMS shows consistent sheet resistance of 386 ± 55 Ω/sq, with up to 300% tensile strain until failure of the PDMS substrate. For comparison, the sheet resistance of graphene on PDMS which dramatically increases for applied tensile strains much smaller than 10%. The sheet resistance measurement shows consistent and low electrical resistivity of the rGO-VACNT hybrid under up to 300% tensile strain.

Fatigue testing of the rGO-VACNT hybrid structure is important for consideration as a component of future flexible electronic devices, which would experience multiple bending and stretching while in use. Cyclic testing of the rGO-VACNT hybrid stretchable electrode is shown in figure 6(b). The rGO-VACNT hybrid on PDMS substrate was manually stretched up to 100% tensile strain (these samples were not stretched to 300% to avoid potential damage to the PDMS substrates) using the stretching stage shown in figure 7, and then released to the original state with no strain applied. Sheet resistances under tensile strain of 0%, 20%, 40%, 80%, and 100% were measured using four-point probe method at the 1st, 5th, 10th, 30th, and 50th cycles. After 50 cycles stretching to 100% tensile strain, the electrode does not show any increase in sheet resistance, indicating its durability under large applied tensile strain conditions.

Due to the measured performance of the rGO-VACNT hybrid in terms of electrical conductivity, maximum strain, and durability, the hybrid electrodes show promise for the use in stretchable and flexible electronics. This is demonstrated with a simple LED circuit shown in figure 7, where the LED bulb and external power supply were electrically connected by a rGO-VACNT hybrid electrode. The LED bulb showed the same light intensity emission with maximum tensile train of 100% applied to the rGO-VACNT hybrid stretchable electrode.

4. Conclusions

In this work we have described the fabrication and characterization of a highly stretchable and conductive rGO-VACNT hybrid electrode. The unique fabrication processes includes a direct delamination transfer method of the VACNT from as grown rigid Si/SiO_2 substrates to flexible PDMS substrates coupled with inkjet printing of GO atop VACNT carpets, followed by thermal reduction of GO to rGO to increase electrical conductivity. Characterization of the manufactured rGO-VACNT demonstrates that the hybrid exhibits consistent electrical resistance up to 300% tensile strain, while multiple cyclic stretching tests of the hybrid electrode up to 100% maximum tensile strain show no

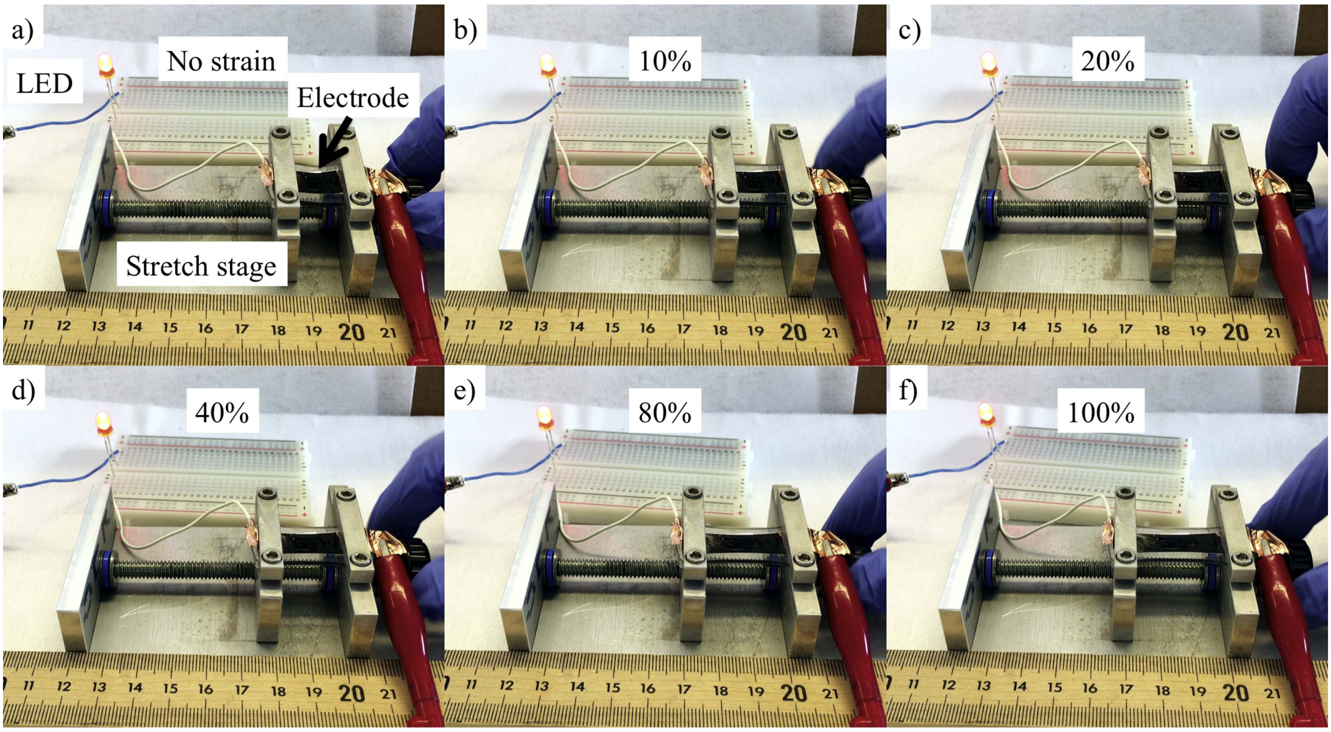

Figure 7. Digital images of the LED powered by an external power supply at consistent voltage with the stretchable electrode operating at 0%–100% tensile strain. (A video for this figure is available.)

increase of sheet resistance. These results suggest that the rGO-VACNT hybrid structure is a promising approach for reliable stretchable electrodes for flexible electronics requiring stable conductivity and subjected to cyclic stretching.

Acknowledgments

This work has been partially carried out in the Micro Device Laboratory (MDL) at Stevens Institute of Technology funded with support from Contract No. W15QKN-05-D-0011. The authors would like to thank Chao Liu at Stevens Institute of Technology for the help of experiment preparation.

ORCID iDs

Junjun Ding https://orcid.org/0000-0002-7025-0617
Eric Boon https://orcid.org/0000-0002-9033-6215
Eui-Hyeok Yang https://orcid.org/0000-0003-4893-1691

References

[1] Fejes D, Pápa Z, Kecsenovity E, Réti B, Toth Z and Hernadi K 2015 *Appl. Phys.* A **118** 855
[2] Rolison D R, Long J W, Lytle J C, Fischer A E, Rhodes C P, McEvoy T M, Bourg M E and Lubers A M 2009 *Chem. Soc. Rev.* **38** 226
[3] Chen Z, Ren W, Gao L, Liu B, Pei S and Cheng H-M 2011 *Nat. Mater.* **10** 424
[4] Estevez L, Dua R, Bhandari N, Ramanujapuram A, Wang P and Giannelis E P 2013 *Energy Environ. Sci.* **6** 1785
[5] Kim N D, Li Y, Wang G, Fan X, Jiang J, Li L, Ji Y, Ruan G, Hauge R H and Tour J M 2016 *Nano Lett.* **16** 1287
[6] Ding J, Fisher F T and Yang E-H 2016 *J. Vac. Sci. Technol.* B **34** 051205
[7] Xue Y, Ding Y, Niu J, Xia Z, Roy A, Chen H, Qu J, Wang Z L and Dai L 2015 *Sci. Adv.* **1** e1400198
[8] Park J *et al* 2016 *Nanoscale* **8** 10591
[9] Kim J, Kim M, Lee M-S, Kim K, Ji S, Kim Y-T, Park J, Na K, Bae K-H and Kim H K 2017 *Nat. Commun.* **8** 14997
[10] Tang J, Liu J, Torad N L, Kimura T and Yamauchi Y 2014 *Nano Today* **9** 305
[11] Chen T, Peng H, Durstock M and Dai L 2014 *Sci. Rep.* **4** 3612
[12] Yokota T, Zalar P, Kaltenbrunner M, Jinno H, Matsuhisa N, Kitanosako H, Tachibana Y, Yukita W, Koizumi M and Someya T 2016 *Sci. Adv.* **2** e1501856
[13] Liang J, Li L, Tong K, Ren Z, Hu W, Niu X, Chen Y and Pei Q 2014 *ACS Nano* **8** 1590
[14] Kim K, Kim J, Hyun B G, Ji S, Kim S-Y, Kim S, An B W and Park J-U 2015 *Nanoscale* **7** 14577
[15] Chauvin A, Delacôte C, Molina-Luna L, Duerrschnabel M, Boujtita M, Thiry D, Du K, Ding J, Choi C-H and Tessier P-Y 2016 *ACS Appl. Mater. Interfaces* **8** 6611
[16] Mel A-A E *et al* 2016 *J. Phys. Chem.* C **120** 17652
[17] Mel A A E, Tessier P Y, Buffiere M, Gautron E, Ding J, Du K, Choi C H, Konstantinidis S, Snyders R and Bittencourt C 2016 *Small* **12** 2885
[18] Thiry D, Molina-Luna L, Gautron E, Stephant N, Chauvin A, Du K, Ding J, Choi C-H, Tessier P-Y and Mel A-A E 2015 *Chem. Mater.* **27** 6374

[19] Wang Z L, Xu D, Xu J J, Zhang L L and Zhang X B 2012 *Adv. Funct. Mater.* **22** 3699
[20] Jiang H, Lee P S and Li C 2013 *Energy Environ. Sci.* **6** 41
[21] Yun Y S, Park M H, Hong S J, Lee M E, Park Y W and Jin H-J 2015 *ACS Appl. Mater. Interfaces* **7** 3684
[22] Kim T, Jung G, Yoo S, Suh K S and Ruoff R S 2013 *ACS Nano* **7** 6899
[23] Singh A P *et al* 2015 *Carbon* **85** 79
[24] Silva T A, Zanin H, Vicentini F C, Corat E J and Fatibello-Filho O 2015 *Sensors Actuators* B **218** 51
[25] Welna D T, Qu L, Taylor B E, Dai L and Durstock M F 2011 *J. Power Sources* **196** 1455
[26] Li S, Luo Y, Lv W, Yu W, Wu S, Hou P, Yang Q, Meng Q, Liu C and Cheng H-M 2011 *Adv. Energy Mater.* **1** 486
[27] Kim U J *et al* 2011 *Adv. Mater.* **23** 3809
[28] Meshot E R, Plata D E L, Tawfick S, Zhang Y, Verploegen E A and Hart A J 2009 *ACS Nano* **3** 2477
[29] Yoku I, Kazumichi N, Yuta M, Takayuki N and Gunther K 2016 *Nanotechnology* **27** 115701
[30] Jiang J, Li Y, Gao C, Kim N D, Fan X, Wang G, Peng Z, Hauge R H and Tour J M 2016 *ACS Appl. Mater. Interfaces* **8** 7356
[31] Inoue Y *et al* 2011 *Carbon* **49** 2437
[32] Hiramatsu M, Deguchi T, Nagao H and Hori M 2007 *Japan. J. Appl. Phys.* **46** L303
[33] Shui J, Wang M, Du F and Dai L 2015 *Sci. Adv.* **1** e1400129
[34] Andričević P, Kollár M, Mettan X, Náfrádi B, Sienkiewicz A, Fejes D, Hernadi K, Forró L and Horváth E 2017 *J. Phys. Chem.* C **121** 13549
[35] Cho W, Schulz M and Shanov V 2014 *Carbon* **72** 264
[36] Li C, Li Z, Zhu H, Wang K, Wei J, Li X, Sun P, Zhang H and Wu D 2010 *J. Phys. Chem.* C **114** 14008
[37] Ding J, Du K, Wathuthanthri I, Choi C-H, Fisher F T and Yang E-H 2014 *J. Vac. Sci. Technol.* B **32** 06FF01
[38] Fan Z, Yan J, Zhi L, Zhang Q, Wei T, Feng J, Zhang M, Qian W and Wei F 2010 *Adv. Mater.* **22** 3723
[39] Zhu Y *et al* 2012 *Nat. Commun.* **3** 1225
[40] Kumar K, Kim Y-S, Li X, Ding J, Fisher F T and Yang E-H 2013 *Chem. Mater.* **25** 3874
[41] Kim Y-S, Kumar K, Fisher F T and Yang E-H 2012 *Nanotechnology* **23** 015301
[42] Yuan W, Zhang Y, Cheng L, Wu H, Zheng L and Zhao D 2016 *J. Mater. Chem.* A **4** 8932
[43] Le L T, Ervin M H, Qiu H, Fuchs B E and Lee W Y 2011 *Electrochem. Commun.* **13** 355
[44] Das S R, Nian Q, Cargill A A, Hondred J A, Ding S, Saei M, Cheng G J and Claussen J C 2016 *Nanoscale* **8** 15870
[45] Secor E B, Prabhumirashi P L, Puntambekar K, Geier M L and Hersam M C 2013 *J. Phys. Chem. Lett.* **4** 1347
[46] Kim J, Kwon S, Cho D-H, Kang B, Kwon H, Kim Y, Park S O, Jung G Y, Shin E and Kim W-G 2015 *Nat. Commun.* **6** 8294
[47] Kang S J, Kocabas C, Kim H-S, Cao Q, Meitl M A, Khang D-Y and Rogers J A 2007 *Nano Lett.* **7** 3343
[48] Tsai T Y, Lee C Y, Tai N H and Tuan W H 2009 *Appl. Phys. Lett.* **95** 013107
[49] Jung Y J, Kar S, Talapatra S, Soldano C, Viswanathan G, Li X, Yao Z, Ou F S, Avadhanula A and Vajtai R 2006 *Nano Lett.* **6** 413
[50] Hofmann S, Ducati C, Kleinsorge B and Robertson J 2003 *Appl. Phys. Lett.* **83** 4661
[51] Huh S H 2011 Thermal reduction of graphene oxide *Physics and Applications of Graphene - Experiments* (Rijeka: Intech) (https://doi.org/10.5772/14156)
[52] Johnston I, McCluskey D, Tan C and Tracey M 2014 *J. Micromech. Microeng.* **24** 035017
[53] Yang D, Velamakanni A, Bozoklu G, Park S, Stoller M, Piner R D, Stankovich S, Jung I, Field D A and Ventrice C A 2009 *Carbon* **47** 145
[54] Sobon G, Sotor J, Jagiello J, Kozinski R, Zdrojek M, Holdynski M, Paletko P, Boguslawski J, Lipinska L and Abramski K M 2012 *Opt. Express* **20** 19463
[55] Zhu Y, Murali S, Cai W, Li X, Suk J W, Potts J R and Ruoff R S 2010 *Adv. Mater.* **22** 3906
[56] Smits F M 1958 *Bell Syst. Tech. J.* **37** 711